J. Fluid Mech. (1990), *vol.* 217, *pp.* 421–440
Printed in Great Britain

Laminar secondary flows in curved rectangular ducts

By S. THANGAM AND N. HUR
Department of Mechanical Engineering, Stevens Institute of Technology, Hoboken, NJ 07030, USA

(Received 1 July 1988 and in revised form 23 January 1990)

The occurrence of secondary flow in curved ducts due to the centrifugal forces can often significantly influence the flow rate. In the present work, the secondary flow of an incompressible viscous fluid in a curved duct is studied by using a finite-volume method. It is shown that as the Dean number is increased the secondary flow structure evolves into a double vortex pair for low-aspect-ratio ducts and roll cells for ducts of high aspect ratio. A stability diagram is obtained in the domain of curvature ratio and Reynolds number. It is found that for ducts of high curvature the onset of transition from single vortex pair to double vortex pair or roll cells depends on the Dean number and the curvature ratio, while for ducts of small curvature the onset can be characterized by the Dean number alone. A comparison with the available theoretical and experimental results indicates good agreement. A correlation for the friction factor as a function of the Dean number and aspect ratio is developed and is found to be in good agreement with the available experimental and computational results for a wide range of parameters.

1. Introduction

The study of viscous flow in curved (or helically coiled) ducts is of fundamental interest in fluid mechanics. There are numerous applications, which include the flows through turbomachinery blade passages, aircraft intakes, diffusers, and heat exchangers. Some of these problems of practical interest involve strong secondary flows due to longitudinal curvature in the geometry. The presence of longitudinal curvature generates centrifugal forces which act at right angles to the main flow and produce a secondary flow. This causes a reduction in flow rate due to a decrease in the average axial velocity. In addition, the axial velocity profile is distorted (from the quasi-parabolic structure which is characteristic of pressure-driven flows in straight ducts) with an outward shift of the peak axial velocity.

The existing works on laminar flows in curved pipes can be essentially separated into analytical, experimental and computational studies dealing with developing and fully developed flows in circular and non-circular tubes. The earliest studies on curved pipes to predict the onset of secondary flows and its characteristics were by Dean (1927, 1928). His studies showed that the centrifugal effects introduced by the curvature of the pipe cause a pair of counter-rotating vortices to evolve. Since then several analytical, computational and experimental studies have considered different aspects of this important process in detail. The present study considers a subset of this physical process, namely, the fully developed laminar flow of an incompressible viscous fluid in curved rectangular ducts driven by a fixed axial pressure gradient under steady conditions.

Fully developed viscous flows in curved ducts have been shown to depend on the curvature ratio and the Dean number (defined in (3.4)). Past work on fully developed flow in curved square ducts includes numerical studies by Mori, Uchida & Ukon (1971) who obtained a numerical solution by using the boundary-layer approximation (valid for large Dean numbers); Cheng, Lin & Ou (1976), Ghia & Sokhey (1977), and Joseph, Smith & Adler (1975) who obtained solutions which predicted the existence of a weak second vortex pair near the outer wall above a certain value of the Dean number. This second vortex pair was found to rotate in the opposite manner to the primary vortex pair. Cheng *et al.* (1976) predicted the onset of the second vortex pair to occur above a Dean number of 150, Ghia & Sokhey predicted it to occur above a Dean number of 143, while the calculations of Joseph *et al.* give a threshold Dean number of 152. (Here, and elsewhere in this work, to avoid confusion stemming from the definitions of Dean number employed by different authors, all published values have been converted using the definition in (3.4)). However, since the curvature ratio (whose effect is embedded in the Dean number) may itself play an important role for highly curved ducts, the suitability of the Dean number as the sole parameter to characterize the onset of the second vortex pair is unclear.

Experiments on the flow in curved square ducts have been performed by Baylis (1971), Mori *et al.* (1971), Humphrey, Taylor & Whitelaw (1977), and Hille, Verenkamp & Schulz-Dubois (1985). Baylis (1971) obtained the friction factors for the range of Dean numbers $500 < De < 70000$ and the curvature ratio $1.75 < C < 17.5$ and gave an empirical correlation for the friction factor in terms of the Dean number. Mori *et al.* (1971) measured axial velocity profiles at the midplane of the cross-section for $28 < De < 2517$ at $C = 14$ and Humphrey *et al.* (1977) used laser-Doppler anemometry for developing flow at a Dean number of 368 and the curvature ratio of 4.6. Hille *et al.* (1985) also used laser-Doppler anemometry, for $C = 6.45$, and gave a detailed description of the structure of the secondary flow. They were also able to predict the onset of the second vortex pair in the range $150 < De < 300$. Kelleher, Flentie & McKee (1980) performed experiments in a high-aspect-ratio duct ($= 40$) using hot-wire anemometry and flow visualization techniques. They observed the multicellular flow at the Dean numbers of 214.7, 257.3, and 307.7 for a curvature ratio of 24.3. They also found that the cell aspect ratio, which is the average ratio of cell height to width, is approximately 0.81 for all three values of the Dean number.

For curved rectangular ducts Cheng *et al.* (1976) performed calculations for duct aspect ratios (defined as the ratio of height H to width B) of 0.5, 2, and 5 for the range of the Dean number 15.9 to 312.7 at curvature ratios of 100 and 30. They reported that, for an aspect ratio of 0.5, at $De = 176$ there were no additional vortices and at $De = 200$ there was a pair of very weak vortices close to the outer wall. In addition, they found that for an aspect ratio of 5, a pair of secondary vortices appeared at a rather low Dean number of 76 and the eye of the primary vortex moved toward the upper and lower walls with the increase of the Dean number. They gave correlations for the friction factor in terms of the Reynolds number and the aspect ratio.

A study by Winters (1987) considers the bifurcation of secondary flow solutions for fully developed laminar flow in curved rectangular ducts. The study is based on finite-element analysis and shows the existence of multiple solutions arising from the nonlinear equations for the range of aspect ratio from 0.8 to 1.6. A recent work by Ravi Sankar, Nandakumar & Masliyah (1988) considers the related problems of developing flow in curved ducts. They have shown that for a range of curvature ratios and Dean numbers the flows develop into previously known two- and four-cell

patterns based on fully three-dimensional calculations using the parabolized form of the Navier–Stokes equations. They have also shown that for loosely coiled ducts (of curvature ratio of 100) outside a narrow range of Dean number the solution exhibits sustained oscillations in the axial direction and that no stable steady solutions could be predicted. This interesting aspect of the evolution of secondary flow in curved ducts requires further investigation and is not considered in detail in the present work. However, a brief discussion on the stability of secondary flows in square ducts of moderate to strong curvature based on some preliminary computations is given in §3.

Since the longitudinal curvature plays a role similar to that of spanwise rotation, a brief review of some recent work on pressure-driven laminar flow in rectangular ducts subject to spanwise rotation will be considered here. It should be noted that in the case of ducts subjected to spanwise rotation, the Rossby number Ro (defined by $Ro = \bar{W}/(2\Omega B)$, where Ω is an angular velocity of the spanwise rotation and B is the width of the channel) plays a role similar to the curvature ratio. A numerical study by Speziale (1982) used a stream function–vorticity formulation based on Arakawa's method to analyse viscous flow for aspect ratios of 2 and 8 in the Reynolds-number range of 0 to 500, and Rossby-number range of 0.1 to 100. His results show that the secondary flow for high rotation number has a double-vortex-pair structure which is similar to the results of Cheng *et al.* (1976) for high-Dean-number flow in curved ducts. Kheshgi & Scriven (1985) solved the problem of pressure-driven flow in a rotating square channel with a finite-element method, and obtained the double-vortex-pair structure along with detailed stability boundaries. They also observed that the two-vortex family of solutions changes to four-vortex solution at an imperfect bifurcation. Speziale & Thangam (1983) considered the roll-cell instabilities for a duct of aspect ratio 8 in the Reynolds-number range of 0 to 500, and Rossby-number range of 0.0001 to 3, by using the stream function–vorticity formulation based on Arakawa's scheme. They characterized the onset and evolution of the roll-cell structure from the two-vortex configuration which occurs at weak-rotation rates. In the present study certain additional features of similarity between pressure-driven laminar flows in curved ducts and in ducts subject to spanwise rotation will be discussed.

The primary focus of the present work will be on the onset and evolution of secondary motion in the fully developed laminar flow of incompressible viscous fluids in curved rectangular ducts driven by a fixed axial pressure gradient at steady conditions. The motivation for the present study arose from the fact that (i) there exists no detailed study of the flow in curved rectangular ducts of high aspect ratio; (ii) the transition in secondary flow structure due to curvature effects has not been fully analysed in the range of parameters of engineering importance; (iii) there are no generalized friction-factor (or flow reduction) correlations. A finite-volume algorithm suitable for handling cylindrical geometry is used to analyse laminar flows in curved ducts for a wide range of aspect ratios. Next, the governing equations and the numerical procedure will be described, and this will be followed by a discussion of the results and the conclusions.

2. Formulation and the method of solution

The problem to be considered is that of fully developed motion of an incompressible viscous fluid in curved ducts of rectangular cross-section. It should be noted that the flow in helically coiled ducts may be also considered as a flow in curved ducts so long

as the ratio of torsion to curvature of a helical duct remains small. With reference to figure 1, the pitch is shown to be $2\pi L$, and the curvature ζ and the torsion ξ are defined as $\zeta = R/(L^2+R^2)$ and $\xi = L/(L^2+R^2)$, where R is the radius of helical coil, which can be approximated as the radius of curvature when L/R is very small. Kao (1987) studied the torsion effect on fully developed flow in helical pipe and found that if the ratio ξ/ζ is of order unity, the presence of torsion can produce a large effect on the flow pattern, but has negligible effect on flow resistance (see also Manlapaz & Churchill 1980).

The flow is steady and primarily generated by a fixed axial pressure gradient. The duct is sufficiently long compared to its base length B and height H so that there exists a central section of the duct where the end effects are negligible and the flow properties are independent of the axial coordinate ϕ. In the limit of infinite curvature ratio $C = R/D_h$ where D_h is the hydraulic diameter, the flow field corresponds to that in straight ducts of rectangular cross-section and the velocity profile is unidirectional and quasi-parabolic. However, for finite curvature ratios, the fully developed velocity field is three-dimensional, i.e. the velocity vector $\boldsymbol{v}$ in a cylindrical coordinate system is of the form

$$\boldsymbol{v} = \{u(r,z), v(r,z), w(r,z)\}, \tag{2.1}$$

where u, v and w denote radial, vertical, and axial velocity, respectively. Here, the u- and v-components of velocity constitute the secondary flow. For the case of laminar motion, the three velocity components and the pressure P are the solutions of the equations for the conservation of mass and momentum:

$$\left.\begin{aligned}
&u_r + v_z + \frac{u}{r} = 0,\\
&uu_r + vu_z - \frac{w^2}{r} = -\frac{1}{\rho}P_r + \nu\left[u_{rr} + \frac{1}{r}u_r + u_{zz} - \frac{u}{r^2}\right],\\
&uv_r + vv_z = -\frac{1}{\rho}P_z + \nu\left[v_{rr} + \frac{1}{r}v_r + v_{zz}\right],\\
&uw_r + vw_z + \frac{uw}{r} = -\frac{1}{\rho r}P_\phi + \nu\left[w_{rr} + \frac{1}{r}w_r + w_{zz} - \frac{w}{r^2}\right],
\end{aligned}\right\} \tag{2.2}$$

where ρ is the density of the fluid, ν is the kinematic viscosity, and the subscripts denote partial differentiation.

The set of equations (2.2) are solved numerically under steady conditions. In this study a finite-volume method is used and the primitive variables (velocities and pressure) are solved for directly. It should be noted that in the finite-volume scheme, the formulation assures the conservation of mass (Patankar 1980). The algorithms used in the present study is a modification of that proposed by Patanakar (1980) to increase its rate of convergence by extracting information of the pressure field from a given velocity field (Hur 1988).

The computational technique is based on semi-implicit line relaxation of a system of algebraic difference equations obtained by expressing the governing equations over a staggered mesh system. For this purpose, the computational domain is discretized into $M \times N$ finite-volume cells. At the centroid of each cell the variables such as the pressure and the axial velocity are defined, whereas the velocities u and v are defined at the horizontal and vertical cell walls, respectively. The details of the difference equation and the algorithms may be found in Hur (1988).

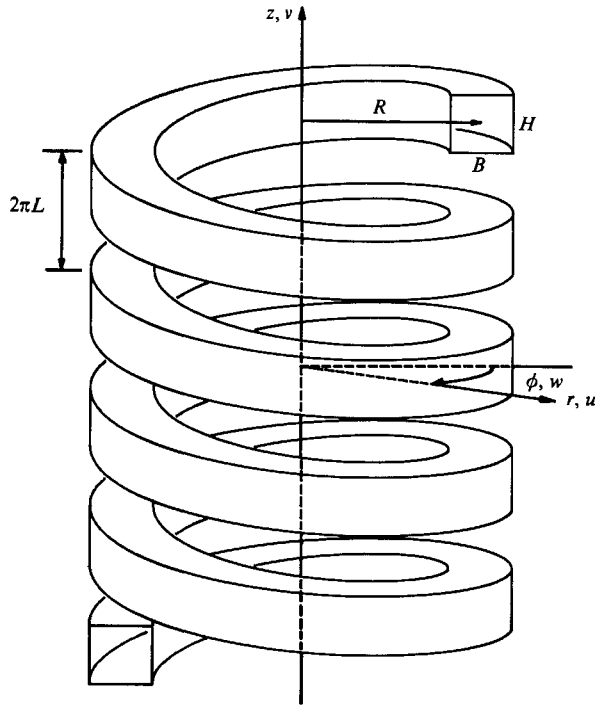

FIGURE 1. Physical configuration and coordinate system of helically coiled duct.

The boundary conditions for the velocities u, v, and w are based on 'no-slip' at the walls. Unlike the stream-function formulation of equations, the primitive-variable formulation discussed herein requires the specification of pressure on the boundary. In the staggered mesh algorithm used in this work, the control volumes on the boundary are located such that one of its sides coincides with the boundary. Since the normal velocity on the boundary is known (in this case based on the 'no-slip' condition) the pressure at the centroid can be obtained from the conservation of mass. Descriptions of the numerical implementation of the boundary conditions for finite-volume schemes can be found in, for example, Roache (1972), Patankar (1980), Hur (1988).

The computations reported in this study were carried out using a 32×32 mesh for square ducts, a 32×64 mesh for 1×2 rectangular ducts, a 32×128 mesh for 1×4 rectangular ducts and a 16×128 and 32×256 mesh for 1×8 rectangular ducts. This mesh scheme was selected based on a detailed study of the adequate resolution of the primitive variables for the range of parameters considered. Typically, the computations were started for a selected aspect ratio and Reynolds number using the results from the straight-duct flow (i.e. the quasi-parabolic profile) as the initial solution. The calculations were performed iteratively using a semi-implicit line-relaxation procedure, and the solution was assumed to be converged in a numerical sense if the average relative error in each of the primitive variables (i.e. velocity components and the pressure) is less than 10^{-5} (0.001%) between successive iterations. The curvature ratio was then increased in small steps with the converged solutions from the previous curvature ratio acting as the initial solution for the computations. The calculations were then repeated for different aspects ratios and Reynolds numbers. In order to improve the speed of convergence to steady solutions

for ducts of moderate to high curvature ratio (tightly coiled ducts), the computations were performed using an implicit time-marching method starting from an initial state consisting of converged solutions from an adjacent parameter set. In addition, the procedure was used to verify that the solutions obtained were not dependent upon the initial conditions.

3. Results and discussion

To facilitate the discussion of the results, the governing equations are first put into dimensionless form. The bulk mean axial velocity of the fluid in a straight duct, W_0, corresponding to a specified pressure gradient is used as the velocity scale, and the hydraulic diameter, D_h is used as the lengthscale. The scaled variables are

$$\left.\begin{aligned} \hat{u} &= \frac{u}{W_0}, \quad \hat{v} = \frac{v}{W_0}, \quad \hat{w} = \frac{w}{W_0}, \quad \hat{P} = \frac{P}{\rho W_0^2}, \\ \hat{t} &= \frac{tW_0}{D_h}, \quad \hat{r} = \frac{r}{D_h}, \quad \hat{z} = \frac{z}{D_h}. \end{aligned}\right\} \tag{3.1}$$

It should be noted that $D_h = 0.5H/(A+1)$, where $A = H/B$ is the aspect ratio of the duct. The dimensionless governing equations based on these variables are given by (after omitting $\hat{}$ for convenience)

$$\left.\begin{aligned} &\frac{1}{r}(ru)_r + v_z = 0, \\ &\frac{1}{r}(ru^2)_r + (uv)_z = \frac{1}{Re_s}\left[\frac{1}{r}(ru_r)_r + u_{zz} - \frac{u}{r^2}\right] - P_r + \frac{w^2}{r}, \\ &\frac{1}{r}(ruv)_r + (v^2)_z = \frac{1}{Re_s}\left[\frac{1}{r}(rv_r)_r + v_{zz}\right] - P_z, \\ &\frac{1}{r}(ruw)_r + (vw)_z = \frac{1}{Re_s}\left[\frac{1}{r}(rw_r)_r + w_{zz} - \frac{w}{r^2}\right] - \frac{1}{r}P_\phi - \frac{uw}{r}. \end{aligned}\right\} \tag{3.2}$$

Here, the coordinate-variable subscripts (r, z, ϕ) denote partial differentiation, and Re_s is the Reynolds number based on the bulk mean velocity in a straight duct, i.e.

$$Re_s = \frac{W_0 D_h}{\nu}. \tag{3.3}$$

In order to evaluate the volumetric flow reduction due to the presence of the curvature, it is convenient to define a modified Reynolds number based on the bulk mean velocity of fully developed flow in curved ducts. The curvature ratio will be defined as the ratio of the radius of curvature of a duct to the hydraulic diameter. Because we have used the hydraulic diameter as a lengthscale for the radial coordinate r, the curvature ratio does not appear in the equations explicitly. The curvature ratio, however, is a necessary parameter for the analysis of flow in curved ducts. The Dean number can then be defined based on the modified Reynolds number, Re, and the curvature ratio, C:

$$Re = \frac{\bar{W} D_h}{\nu}, \quad C = \frac{R}{D_h}, \quad De = Re\, C^{-0.5}. \tag{3.4}$$

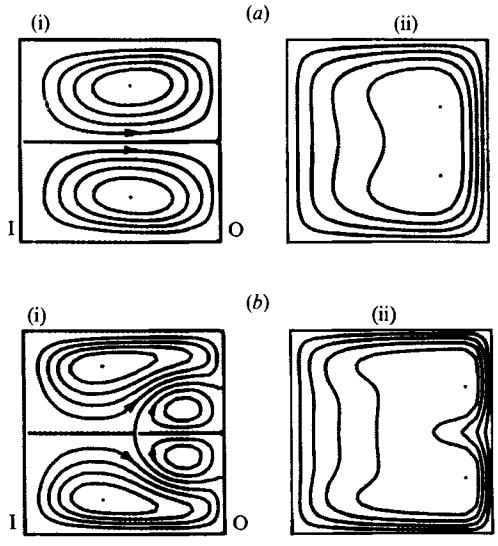

FIGURE 2. (i) Secondary flow streamlines and (ii) axial velocity contours in a curved square duct for $C = 2.5$, illustrating the transition from a single vortex to double vortex pair (I and O represent the inner and outer sidewalls, respectively, here and in subsequent figures.) (*a*) $Re = 126$ ($De = 80$), (*b*) $Re = 284$ ($De = 179$).

It should be noted that by definition (and to conform with existing literature on curved ducts), small curvature ratio represents ducts of high curvature (i.e. tightly coiled), and large curvature ratio represents ducts of low curvature (i.e. loosely coiled).

The system of equations (3.2) was discretized based on a finite-volume scheme and solved for steady-state conditions by using a semi-implicit procedure as discussed in §2. The results for laminar incompressible flow of viscous fluids in curved ducts of aspect ratio 1, 2, 4, and 8 were obtained for a range of Dean numbers and curvature ratios of interest, and are shown in figures 2–13.

In figure 2, the streamlines and axial-velocity contours are shown for a square duct of curvature ratio 2.5 at two different Reynolds numbers. As can be seen from figure 2(*a*), for $Re = 126$ ($De = 80$) two counter-rotating vortices are present (with the upper vortex in counterclockwise and the lower one in clockwise motion). The point where the maximum of the axial velocity occurs is shifted towards the outer wall owing to the centrifugal force. In these and in the following figures, the symbols I and O represent the inner and outer sidewalls, respectively.

When the Reynolds numbers is increased to 284 ($De = 179$), a pair of additional vortices appears which rotates in the opposite sense to the main vortices (figure 2*b*). The imbalance between the pressure gradient and the centrifugal force causes the transition from the single-vortex-pair to the double-vortex-pair structure. This causes the location of the maximum axial velocity to move near the outer wall in symmetrical positions above and below the radial centreline. In the region near the centre of the outer wall, the pressure gradient across the duct in the radial direction is positive but the centrifugal force decreases from a maximum value to zero at the outer wall.

It should be noted here that the Dean number at which this transition occurs has been predicted by Joseph *et al.* (1975), Cheng *et al.* (1976), and Ghia & Sokhey (1977) as 152, 150 and 143, respectively. The discrepancies are because the transition is not

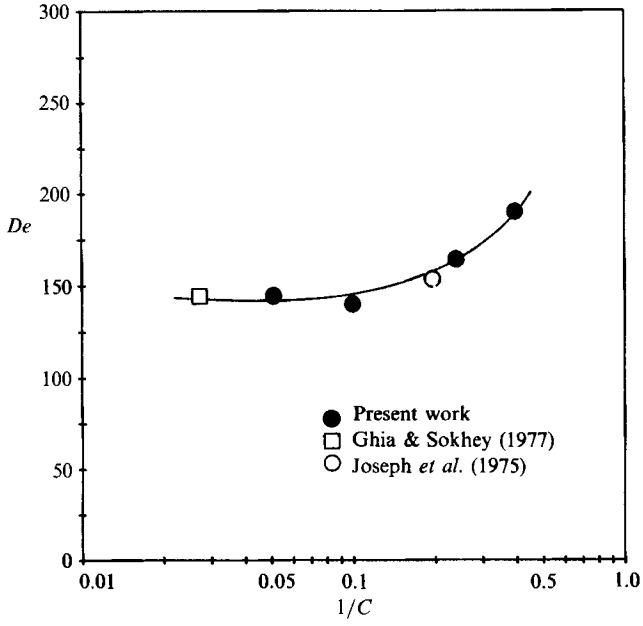

FIGURE 3. Stability diagram in Dean number – curvature ratio plane for a square duct. (The region below the curve represents a single vortex pair while the region above the curve represents a double-vortex-pair secondary flow.)

a function of the Dean number alone for small curvature ratios (that is, for the case of highly curved ducts). To illustrate this, a stability diagram in the Dean number–curvature ratio plane has been developed through a regression analysis of the available data and shown in figure 3. In this diagram, the region below the stability (or transition) curve represents single-vortex-pair secondary flow structure, while the region above the curve corresponds to the double-vortex-pair structure. As can be seen, when the curvature ratio of the duct increases (i.e. for decreasing curvature) the onset of instability (or transition) becomes essentially independent of the curvature ratio. On the other hand, for small values of curvature ratio (i.e. for ducts of high curvature) the onset of instability is a strong function of the curvature ratio and the Dean number.

In figure 4 the secondary flow intensity (defined as the ratio of the maximum secondary flow velocity to the bulk mean axial velocity) is shown as a function of the Dean number for various curvature ratios. As can be seen, the secondary flow intensity varies weakly with the Dean number except near the onset of transition from the single- to double-vortex-pair mode, at which point there is a sudden decrease in the intensity. This decrease in the secondary flow intensity is attributed to the fact that when the flow evolves from a single vortex pair to a counter-rotating double-vortex-pair structure, the maximum secondary flow velocity is reduced. On the other hand, it is seen to be a strong function of the curvature ratio, since the secondary flow is induced by the centrifugal force whose strength is considerably affected by the axial flow velocity.

A point that should be taken into account concerns the stability of the four-vortex secondary flow. Winters (1987) obtained a set of stable and unstable solutions based on a finite-element method for the fully developed flow field in a curved square duct and indicated clearly that the four-vortex symmetric flow can become unstable for

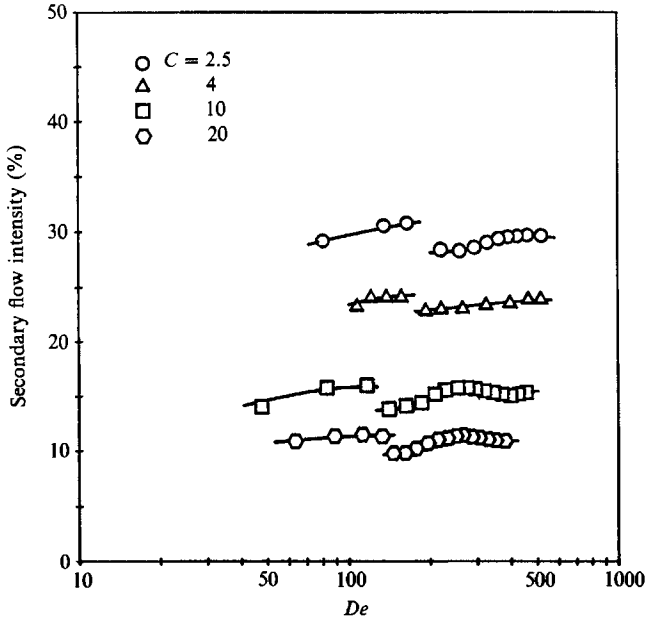

FIGURE 4. Secondary flow intensity as a function of Dean number for square ducts of different curvature ratios.

certain parameter values. Most of the analysis reported by him dealt with loosely coiled ducts with curvature ratios ≈ 50, wherein the secondary flows are quite weak. A recent work by Ravi Sanker *et al.* (1988) considers the time-dependence of the developing flow field in curved square ducts based on the parabolized Navier–Stokes equations. They point out that for loosely coiled ducts there is a range of Dean number for which the flow is characterized by stable solutions and outside this range the solutions can become oscillatory for asymmetric perturbations. Their results also indicate that for tightly coiled ducts both the stable four-vortex and the stable two-vortex solutions exist, and that the four-vortex solution can become unsteady for certain parametric ranges when finite asymmetric perturbations are imposed.

It should be noted that while such detailed analysis were not performed in the present work a series of computations was carried out for a selected set of parameters for square ducts of moderate to strong curvature by solving the time-dependent Navier–Stokes equations. For these computations the four-vortex secondary flow field was first obtained by solving the steady form of the Navier–Stokes equations at suitably selected values of the Dean number and curvature ratio (in the range of $250 \leqslant De \leqslant 525$ and $3 \leqslant C \leqslant 10$). The four-vortex secondary flow was then perturbed and the resulting flow field was used as the initial condition for the time-dependent computations. Two types of perturbations were used: in the first, the four-vortex secondary flow was disturbed in a random manner with the maximum amplitude of the disturbances at 100% of the average amplitude of the undisturbed flow, and the corresponding axial velocity was disturbed in a random manner with the maximum amplitude maintained at 10% of the average amplitude of the undisturbed flow; in the second type, the axial velocity alone was selectively perturbed at 10% of the average amplitude of the undisturbed flow in the upper half of the cross-section. In both cases, the computations were carried out for a large number of time steps using an explicit time-dependent full-mode finite-difference procedure (Roache 1972) and

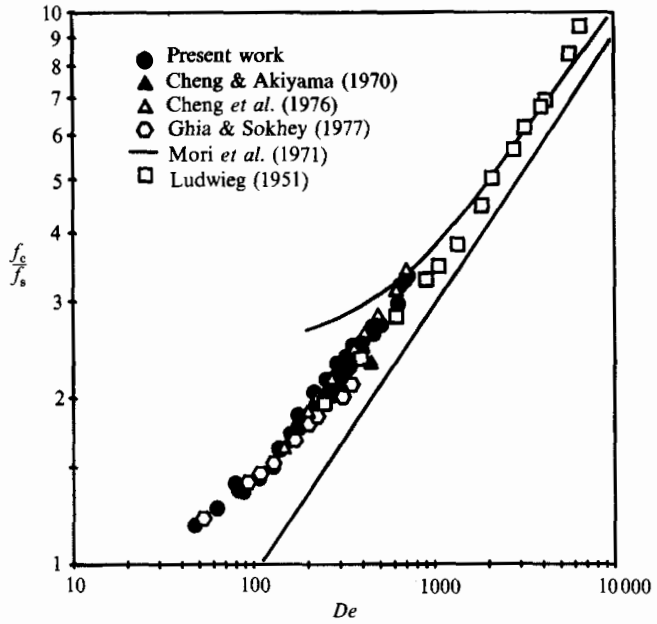

FIGURE 5. Variation of friction factor with Dean number for a square duct – a comparison of present results with available experimental and computational findings.

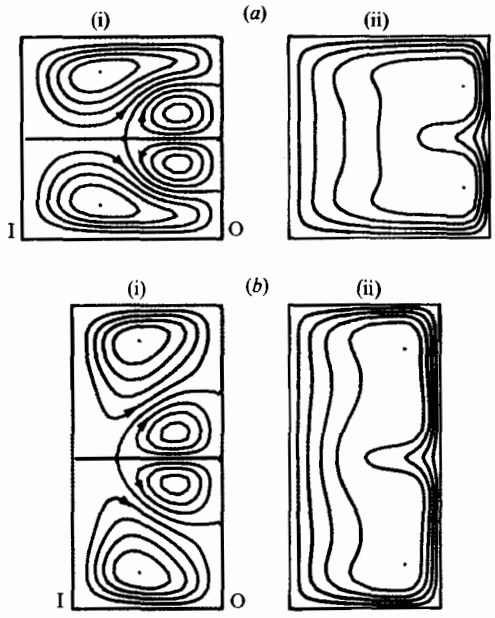

FIGURE 6(*a*, *b*). For caption see facing page.

it was found that the flow field relaxes back to the four-vortex structure obtained from the steady computations. While these do not offer validation that the four-vortex solution is always stable, it is felt that the magnitude of perturbation required to destabilize the flow needs to be much larger. A careful and thorough large-amplitude bifurcation study is required to provide physical insight into this interesting phenomenon.

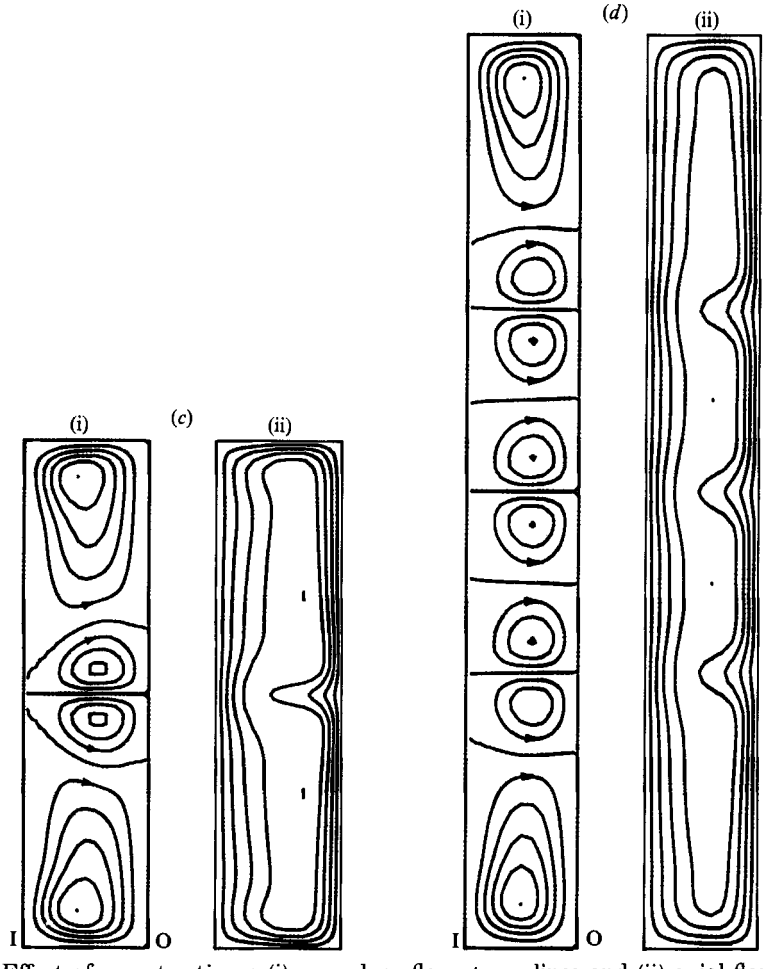

FIGURE 6. Effect of aspect ratio on (i) secondary flow streamlines and (ii) axial flow velocity for $C = 20$. (*a*) $A = 1$, $Re = 798$, $De = 178$; (*b*) $A = 2$, $Re = 919$, $De = 205$; (*c*) $A = 4$, $Re = 1024$, $De = 229$; (*d*) $A = 8$, $Re = 556$, $De = 124$.

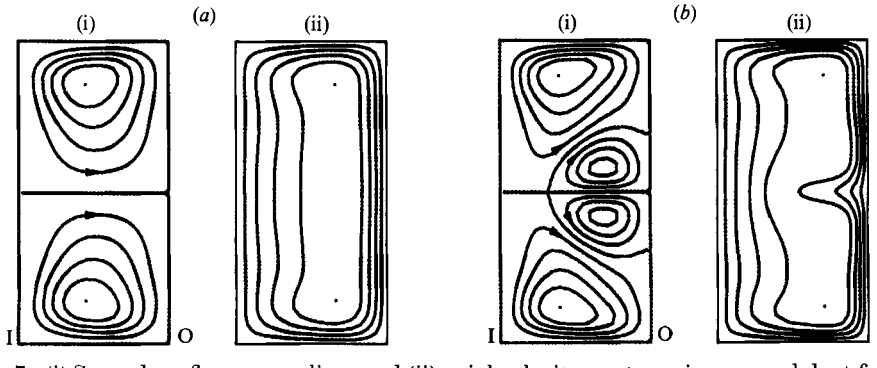

FIGURE 7. (i) Secondary flow streamlines and (ii) axial velocity contours in a curved duct for $A = 2$ and $C = 5$ illustrating the transition from a single vortex to a double vortex pair. (*a*) $Re = 434$ ($De = 194$), (*b*) $Re = 562$ ($De = 251$).

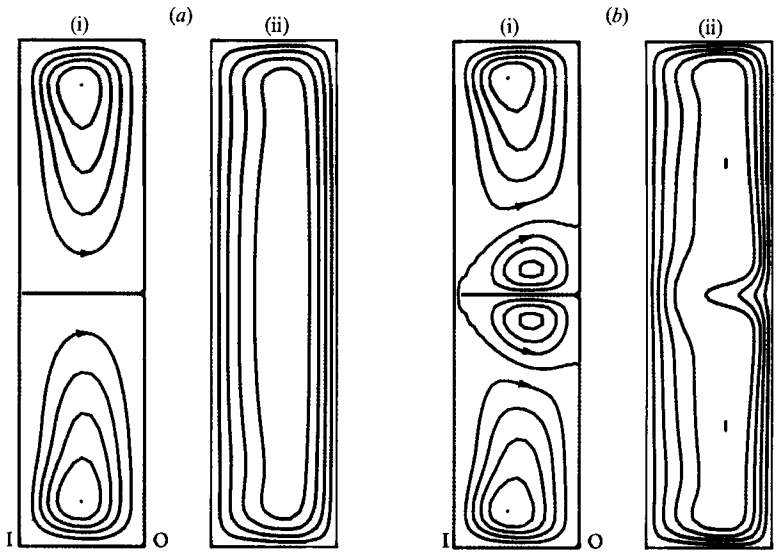

FIGURE 8. (i) Secondary flow streamlines and (ii) axial velocity contours in a curved duct for $A = 4$ and $C = 5$ illustrating the transition from a single vortex to a double vortex pair. (*a*) $Re = 312$ ($De = 140$), (*b*) $Re = 487$ ($De = 218$).

Perhaps the most important result for engineering applications is the estimation of the friction factor (or flow-rate reduction) for the curved ducts. This is especially important when considering the fact that, unlike in straight ducts, the flow rate for the given pressure drop in curved ducts is not known *a priori*. In figure 5 computed values of the friction-factor ratio, f_c/f_s (defined as the ratio of the bulk mean axial velocity of the straight duct to that of the curved duct corresponding to a given pressure drop) for a square duct is shown as a function of the Dean number. The monotonic increase in the friction factor with Dean number shows that an increase in either the axial velocity or curvature causes an increase in the intensity of secondary flow leading to a decrease in flow rate. As can be seen, excellent agreement with earlier experimental and numerical results is present. It should be noted that the friction-factor ratio may be also expressed as

$$\frac{f_c}{f_s} = \frac{Re_s}{Re}. \tag{3.5}$$

The effect of aspect ratio on the flow field is analysed next. In the figure 6(*a–d*), the secondary flow structure is shown for aspect ratios of 1, 2, 4 and 8 at a curvature ratio of 20. It can be seen that, when the aspect ratio is increased, the secondary flow field changes from the double-vortex-pair structure to the roll-cell pattern. To illustrate the onset of instability in ducts of aspect ratio other than one, the flow patterns before and after the instability are shown in figures 7 and 8 for $A = 2$ and 4, respectively. It can be seen here that when $A = 4$ the second vortex pair at the onset of instability spans nearly the entire width of the channel.

In figure 9(*a*, *b*), the flow pattern during the evolution of the instability is shown for an aspect ratio of 8. At low Dean numbers of 22 and 86, only a pair of vortices near the upper and lower walls has been observed. At $De = 107$, two additional weak vortices appear in the centreplane near the outer wall as in the case of the square duct. When the Dean number is further increased to 120, the entire duct is filled with

roll cells. This secondary flow pattern is marked by the presence of four pairs of counter-rotating vortices, which has not been predicted in earlier computational works. In this case, an average cell aspect ratio ($= H_c/B$, where H_c is the average size of the vortex cells neglecting the ones near the top and bottom walls) has been found to be 0.80. This is in good agreement with the experiment of Kelleher *et al.* (1980) where a cell aspect ratio of 0.81 was obtained for the cases of $A = 40$, $C = 24.3$, at $De = 214.7$, 257.3, and 307.7.

It is interesting to note here that the points of local maxima and minima in axial velocity are associated with the boundaries of the two counter-rotating vortices of the secondary flow. This is because at the local maximum or minimum of the axial velocity, the centrifugal force is also at its local maximum or minimum, respectively, and this leads to the formation of the pairs of counter-rotating vortices. These results have striking similarity to the flow pattern observed in ducts of high aspect ratio which are subject to spanwise rotation (e.g. Speziale & Thangam 1983). This is because the contribution to the body force due to centrifugal effects in curved ducts and that from the Coriolis effects in rotating ducts are quite similar (for details, see the Appendix).

The roll-cell instabilities in rotating ducts have been analysed by earlier researchers. Hart (1971) and Lezius & Johnston (1976) obtained the stability boundary based on a linear stability analysis for rotating channel flow, while Speziale & Thangam (1983) obtained this stability boundary by numerically solving the entire nonlinear equations of motion for a rotating duct of aspect ratio 8. Hart (1971) and Lezius & Johnston (1976) also conducted experiments in channels of finite aspect ratio, and verified their computational findings. In order to compare the stability of the flow in curved ducts with that in a rotating duct, the width of the channel is selected as the lengthscale to be consistent with the works of earlier researchers. Based on the width as the lengthscale the curvature ratio C_B, the Reynolds number Re_B, and the Dean number De_B are defined as

$$C_B = \frac{R}{B}, \quad Re_B = \frac{\bar{W}B}{\nu}, \quad De_B = Re_B(C_B)^{-0.5}. \tag{3.6}$$

These parameters are used in the stability diagram, figure 10 (wherein the curves are obtained by a regression analysis), to show the effects of aspect ratio and curvature ratio. As the aspect ratio increases, the Reynolds number at which the instability occurs decreases; i.e. the onset of instability occurs at a much lower Reynolds number. It is also seen that for the range of aspect ratios considered, the effect of an increase of curvature ratio is to cause the onset of instability at lower Reynolds numbers. This is due to the increase in the centrifugal force associated with the curvature of the duct.

In figure 11 a comparison of the stability boundary of the flow field in high-aspect-ratio ducts with curvature, and that in ducts subjected to spanwise rotation is shown. As can be seen, the stability boundaries predicted by Hart (1971), Lezius & Johnston (1976) and Speziale & Thangam (1983) agree quite well with those obtained in the present study. For the purposes of this comparison, the inverse of the curvature ratio of ducts is considered to be equivalent to the rotation number for ducts subject to spanwise rotation (see the Appendix for a discussion). As a further consequence of the above analysis, it should be noted that, similar to the findings for rotating channel flow, for curved ducts of aspect ratio greater than 8 the flow can be treated like flow in a curved channel from the stability point of view. In the present

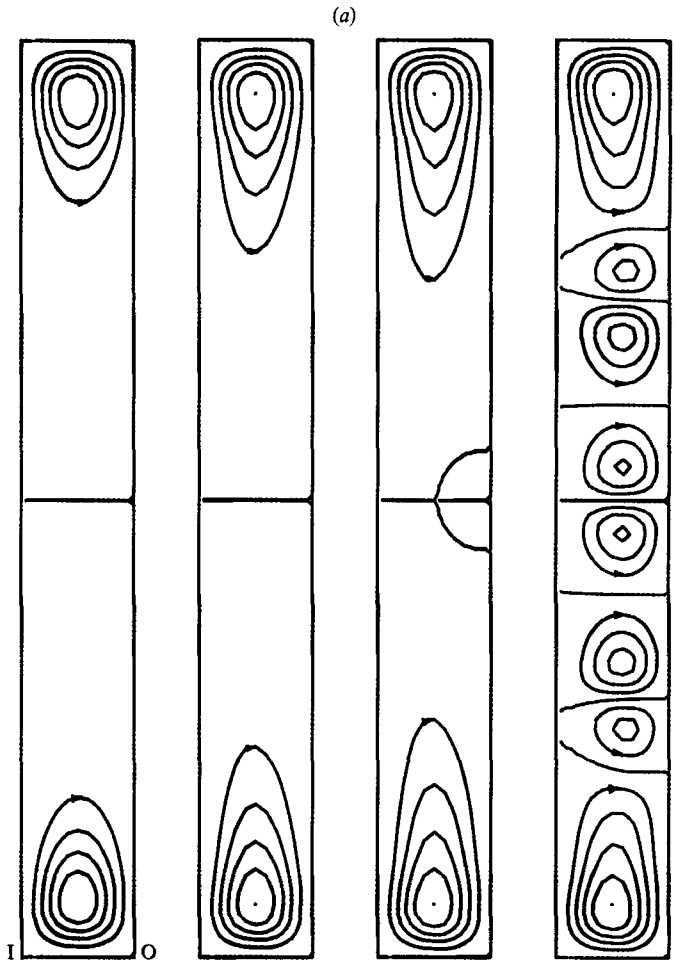

FIGURE 9(a). For caption see facing page.

study, this was independently confirmed by performing computations for ducts of curvature ratio 12 and 16.

In addition,it should be noted (from figures 10 and 11) that the slope of the stability boundary is nearly a constant for high curvature ratios (i.e. for ducts of small curvature). This slope is found to be -0.5, or

$$Re_B(C_B)^{-0.5} = De_B = \text{constant}, \tag{3.7}$$

which confirms the assertion that the transition from a single vortex pair to either a double vortex pair of roll cells is a function of the Dean number alone for ducts of small curvature (or high curvature ratio).

The computed results for the friction-factor ratio, covering a wide range of aspect ratio and Dean number, are given in figure 12. Here, the Dean number is defined based on the hydraulic diameter since this is the lengthscale suitable for determining the friction-factor ratio (or volumetric flow reduction). As can be seen from the figure

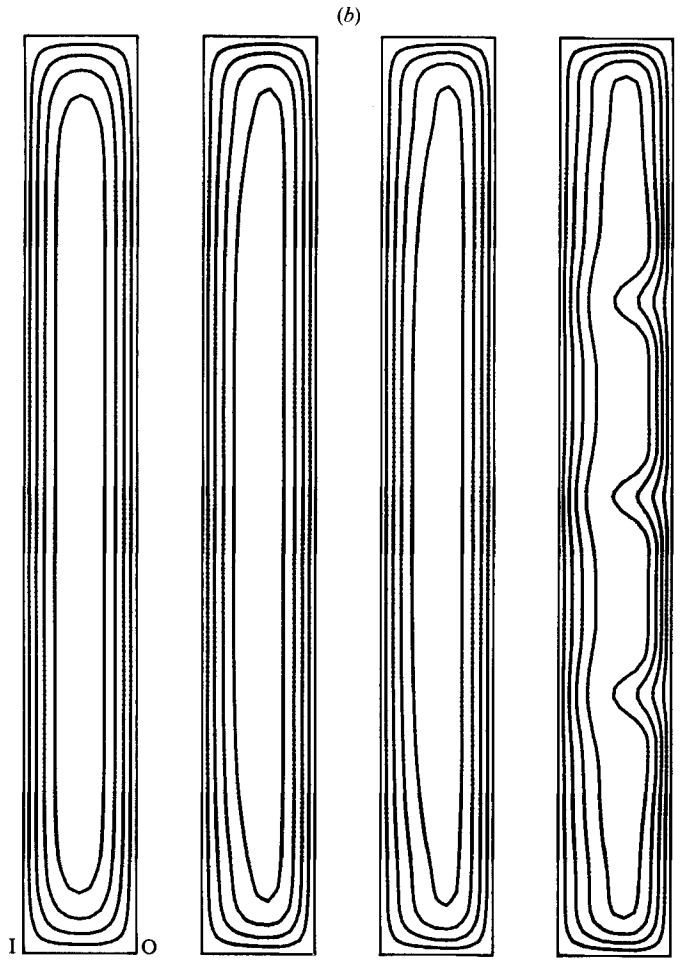

Re = 49	192	239	269
De = 22	86	107	120

FIGURE 9. Evolution of roll-cell instability in a rectangular duct with $A = 8$ and $C = 5$. (*a*) Secondary flow streamlines, (*b*) axial velocity contours.

the friction-factor ratio increases with the Dean number and aspect ratio. Excellent agreement with earlier results is evident from the figure. From an engineering application point of view, there have been efforts to obtain correlations between the friction-factor ratio and Dean number and the aspect ratio. Some well-known correlations available in the literature include:

Baylis (1971):

$$f_c/f_s = 1.51\,De^{\frac{1}{2}}, \quad A = 1 \quad \text{for} \quad 500 < De < 70000, \tag{3.8}$$

Cheng & Akiyama (1970):

$$f_c/f_s = 0.225\,De^{0.39}, \quad A = 1 \quad \text{for} \quad 100 < De < 1500, \tag{3.9}$$

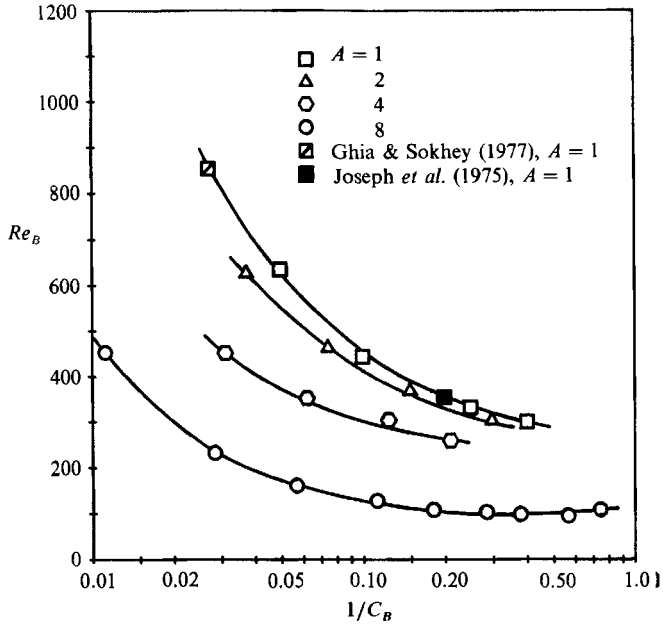

FIGURE 10. Stability diagram for different aspect ratios in the Reynolds number–curvature ratio plane.

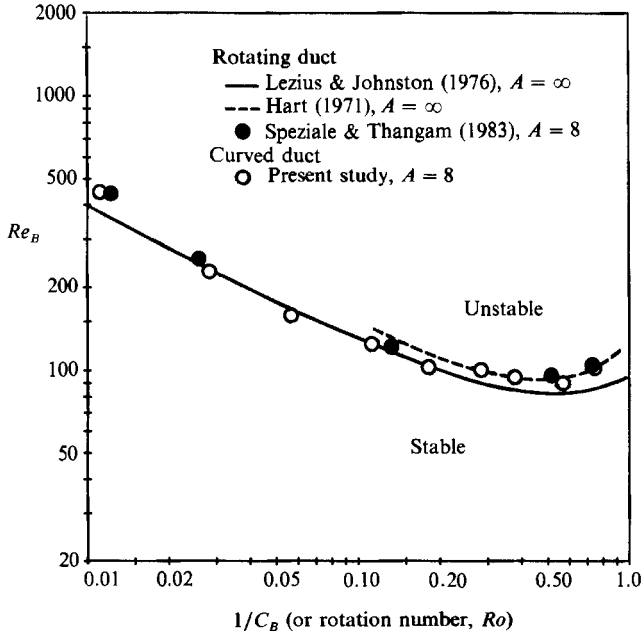

FIGURE 11. Comparison of the stability curve marking the onset of roll-cell instabilities in curved ducts with ducts subject to spanwise rotation.

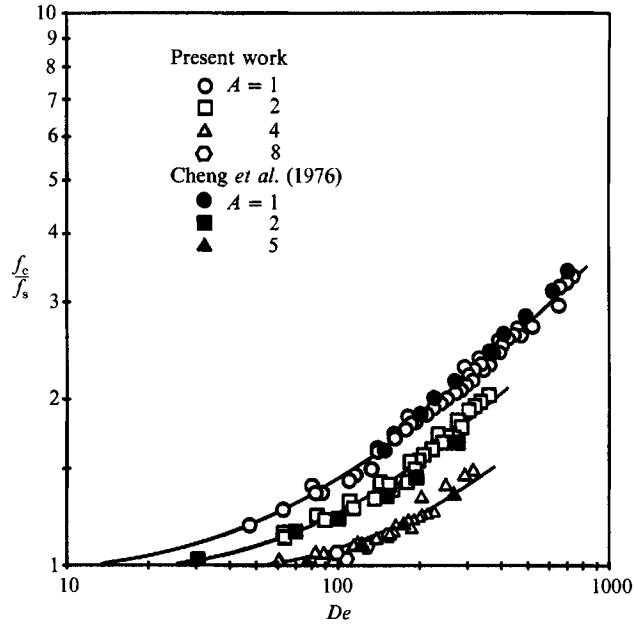

FIGURE 12. Variation of friction factor with Dean number for different aspect ratios – a comparison of present results with available experimental and computational findings.

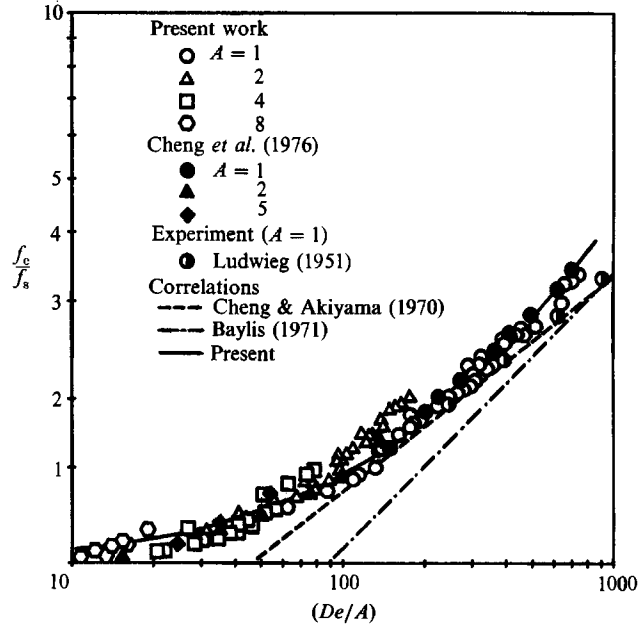

FIGURE 13. Variation of friction factor with modified Dean number for different aspect ratios – a comparison of present results and available experimental and computational findings with the correlation proposed in (3.11).

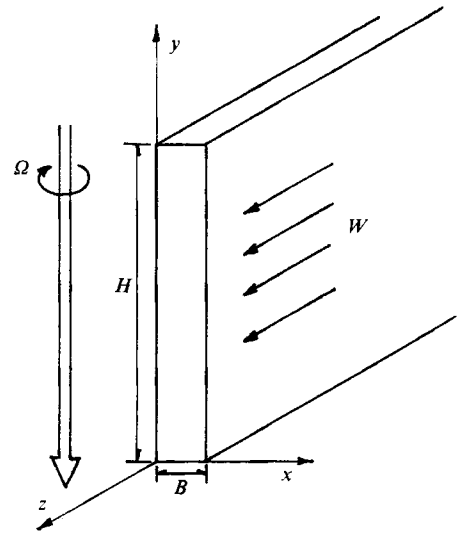

FIGURE 14. Physical configuration and coordinate system for flow in ducts subject to spanwise rotation.

Cheng *et al.* (1976):

$$f_c/f_s = C_0 De^{\frac{1}{2}}(1 + C_1 De^{-\frac{1}{2}} + C_2 De^{-1} + C_3 De^{-\frac{3}{2}} + C_4 De^{-2})$$

where

A	C_0	C_1	C_2	C_3	C_4
1	0.1278	−0.257	0.669	187.7	−512.2
2	0.2736	−24.79	325.2	−1591	2728
5	0.0805	−5.218	104.4	−202.8	0
0.5	0.0974	4.366	−13.56	131.8	−182.6

(3.10)

In the present study the following correlation covering a wide range of parameters is proposed based on a single parameter, namely, the modified Dean number defined as De/A:

$$f_c/f_s = 1 + 0.086\,(\mathrm{De/A})^{0.86}. \tag{3.11}$$

To illustrate the effectiveness of the proposed correlation, in figure 13 the friction-factor ratio is plotted against the modified Dean number along with the results from the present computations as well as those of earlier researchers. As can be seen the correlation gives a good approximation for the range of parameters $10 \leqslant De \leqslant 1000$ and $1 \leqslant A \leqslant 8$. It should also be noted that, unlike the earlier correlations, equation (3.11) also yields the correct limit of $f_c/f_s \to 1$ for $De \to 0$.

4. Conclusions

A detailed numerical study of the onset and evolution of secondary flows in curved rectangular ducts has been conducted using the finite-volume method. The onset of secondary motion is found to be a function of the Dean number and curvature ratio for ducts of high curvature, while for ducts of low curvature the onset can be characterized by the Dean number alone. A comparison with available theoretical and experimental results indicates good agreement. The analogy between pressure-driven laminar flows in curved ducts and straight ducts subject to spanwise rotation

has been demonstrated. A correlation between the friction factor (or reduction in volume flux) and the aspect ratio in terms of a modified Dean number (defined as Dean number over aspect ratio) has been proposed. This has been found to be valid over a wide range of Dean numbers and aspect ratios.

Appendix. Analogy between flow in curved ducts and flow in ducts subject to spanwise rotation

The governing equations for fully developed isothermal flow in curved ducts based on a cylindrical coordinate system consist of (with the subscripts denoting partial derivatives):

$$\left.\begin{aligned}
&\frac{1}{r}(ru)_r + v_z = 0,\\
&\frac{1}{r}(ru^2)_r + (uv)_z = \nu\left[\frac{1}{r}(ru_r)_r + u_{zz} - \frac{u}{r^2}\right] - \frac{1}{\rho}P_r + \frac{w^2}{r}\\
&\frac{1}{r}(ruv)_r + (v^2)_z = \nu\left[\frac{1}{r}(rv_r)_r + v_{zz}\right] - \frac{1}{\rho}P_z,\\
&\frac{1}{r}(ruw)_r + (vw)_z = \nu\left[\frac{1}{r}(rw_r)_r + w_{zz} - \frac{w}{r^2}\right] - \frac{1}{\rho r}P_\phi - \frac{uw}{r}.
\end{aligned}\right\} \tag{A 1}$$

On the other hand, for fully developed viscous flow in ducts subject to spanwise rotation based on a Cartesian coordinate system (see figure 14), the governing equations can be written as

$$\left.\begin{aligned}
&u_x + v_y = 0,\\
&(u^2)_x + (uv)_y = \nu[u_{xx} + u_{yy}] - \frac{1}{\rho}P_x + 2\Omega w,\\
&(uv)_x + (v^2)_y = \nu[v_{xx} + v_{yy}] - \frac{1}{\rho}P_y,\\
&(uw)_x + (vw)_y = \nu[w_{xx} + w_{yy}] - \frac{1}{\rho}P_z - 2\Omega u.
\end{aligned}\right\} \tag{A 2}$$

The sets of equations (A 1) and (A 2) are similar except for the source terms. The source term for secondary flow in a curved duct is the centrifugal force term w^2/r, and that in a rotating duct is the Coriolis force term $2\Omega w$. Therefore, in this analogy the quantity 2Ω in ducts subject to spanwise rotation and the term w/r in curved ducts are expected to have a similar effect on the secondary flow.

The rotation number is a dimensionless parameter appearing in the analysis of flow in ducts subject to spanwise rotation and is defined as

$$Ro = 2\Omega B/W_0 \tag{A 3}$$

This is analogous to the inverse of the curvature ratio for curved ducts:

$$C_B^{-1} = B/R. \tag{A 4}$$

Hence, the comparisons between flow in curved ducts and flow in ducts subject to spanwise rotation can be established based on these two dimensionless parameters.

REFERENCES

BAYLIS, J. A. 1971 Experiments on laminar flow in curved channels of square sections. *J. Fluid Mech.* **48**, 417–422.

CHENG, K. C. & AKIYAMA, M. 1970 Laminar forced convection heat transfer in curved rectangular channels. *Intl J. Heat Mass Transfer* **13**, 471–490.

CHENG, K. C., LIN, R. C. & OU, J. W. 1976 Fully developed laminar flow in curved rectangular channels. *Trans. ASME* I: *J. Fluids Engng* **98**, 41–48.

DEAN, W. R. 1927 Note on the motion of fluid in a curved pipe. *Phil. Mag.* **4**, 208–223.

DEAN, W. R. 1928 The streamline motion of fluid in a curved pipe. *Phil. Mag.* **5**, 673–695.

GHIA, K. N. & SOKHEY, J. S. 1977 Laminar incompressible viscous flow in curved ducts of regular cross-sections. *Trans. ASME* I: *J. Fluids Engng* **99**, 640–648.

HART, J. E. 1971 Instability and secondary motion in a rotating channel flow. *J. Fluid Mech.* **45**, 341–351.

HILLE, P., VEHRENKAMP, R. & SCHULZ-DUBOIS, E. O. 1985 The development and structure of primary and secondary flow in a curved square duct. *J. Fluid Mech.* **151**, 219–241.

HUMPHREY, J. A. C., TAYLOR, A. M. K. & WHITELAW, J. H. 1977 Laminar flow in a square duct of strong curvature. *J. Fluid Mech.* **83**, 509–527.

HUR, N. 1988 Numerical study of secondary flows in curved ducts. Ph.D. thesis, Stevens Institute of Technology.

JOSEPH, B., SMITH, E. P. & ADLER, R. J. 1975 Numerical treatment of laminar flow in helically coiled tubes of square cross section, Part I. Stationary helically coiled tubes. *AIChE J.* **21**, 965–974.

KAO, H. C. 1987 Torsion effect on fully developed flow in a helical pipe. *J. Fluid Mech.* **184**, 335–356.

KELLEHER, M. D., FLENTIE, D. L. & MCKEE, R. J. 1980 An experimental study of the secondary flow in a curved rectangular channel. *Trans. ASME* I: *J. Fluids Engng* **102**, 92–96.

KHESHGI, H. S. & SCRIVEN, L. E. 1985 Viscous flow through a rotating square channel. *Phys. Fluids* **28**, 2968–2979.

LEZIUS, D. K. & JOHNSTON, J. P. 1976 Roll-cell instabilities in rotating laminar and turbulent channel flows. *J. Fluid Mech.* **77**, 153–175.

MANLAPAZ, R. L. & CHURCHILL, S. W. 1980 Fully developed laminar flow in a helically coiled tube of finite pitch. *Chem. Engng Commun.* **7**, 57–78.

MORI, Y., UCHIDA, Y. & UKON, T. 1971 Forced convective heat transfer in a curved channel with a square cross section. *Intl J. Heat Mass Transfer* **4**, 1787–1805.

PATANKAR, S. V. 1980 *Numerical Heat Transfer and Fluid Flow.* McGraw-Hill.

RAVI SANKAR, S., NANDAKUMAR, K. & MASLIYAH, J. H. 1988 Oscillatory flows in coiled square ducts. *Phys. Fluids* **31**, 1348–1359.

ROACHE, P. J. 1972 *Computational Fluid Dynamics.* Hermosa.

SPEZIALE, C. G. 1982 Numerical study of viscous flow in rotating rectangular ducts. *J. Fluid Mech.* **122**, 251–271.

SPEZIALE, C. G. & THANGAM, S. 1983 Numerical study of secondary flows and roll-cell instabilities in rotating channel flow. *J. Fluid Mech.* **130**, 377–395.

WINTERS, K. H. 1987 A bifurcation study of laminar flow in a curved tube of rectangular cross-section. *J. Fluid Mech.* **180**, 343–369.